ChemComm

ROYAL SOCIETY OF CHEMISTRY

COMMUNICATION

Cite this: *Chem. Commun.*, 2022, 58, 10162

Received 28th April 2022,
Accepted 5th August 2022

DOI: 10.1039/d2cc02405e

rsc.li/chemcomm

Photofunctional cyclometallated iridium(III) polypyridine methylsulfone complexes as sulfhydryl-specific reagents for bioconjugation, bioimaging and photocytotoxic applications†

Lili Huang,[a] Peter Kam-Keung Leung,[ab] Lawrence Cho-Cheung Lee,[ac] Guang-Xi Xu,[a] Yun-Wah Lam*[a] and Kenneth Kam-Wing Lo*[ab]

We report herein near-infrared (NIR)-emitting cyclometallated iridium(III) complexes bearing a heteroaromatic methylsulfone moiety as sulfhydryl-specific reagents; one of the complexes was conjugated to cysteine and cysteine-containing peptides and proteins for bioimaging and photocytotoxic applications.

Bioconjugation offers valuable opportunities to label specific biomolecules, such as peptides and proteins, with functional groups for bioimaging and therapeutic applications.[1] Among different amino acids, cysteine is a highly favourable handle for selective conjugation due to its relatively low natural abundance ($<$ 2%) and the highly nucleophilic sulfhydryl side-chain.[2] Recently, heteroaromatic methylsulfones have emerged as a new class of electrophiles for selective sulfhydryl modification *via* nucleophilic aromatic substitution, forming a heteroaryl–thiol linkage in proteins (Scheme 1).[3–7] These methylsulfone-containing reagents display high reactivity and selectivity toward sulfhydryl over other reactive functionalities such as amines, sulfenic acids and *S*-nitrosothiols under mild conditions, compared to widely used thiol-modifying reagents such as maleimide and haloacetamide.[3,5] The reactivity of heteroaromatic methylsulfones toward sulfhydryl can be further enhanced through the introduction of electron-withdrawing groups such as carboxylic acid and nitro moieties.[6] Additionally, the heteroaryl–thiol linkage formed exhibits much higher stability than the thioether linkage in maleimide–thiol conjugates in the presence of acids, bases or external thiols.[4a] Thus, methylsulfone-containing reagents have received considerable attention as labels for peptides and proteins,[4a] for the preparation of antibody–drug conjugates[4b] and for the detection and imaging of thiol species in live cells.[7]

In the past decade, there has been emerging interest in the development of transition metal–peptide conjugates for bioimaging, biosensing and therapeutic applications.[8] Luminescent transition metal complexes such as cyclometallated iridium(III) complexes typically possess many advantages such as their tuneable emission energies, long emission lifetimes, high photostability and high singlet oxygen ($^1O_2$)-photosensitisation capability.[9] These complexes have been conjugated to peptides such as cell-penetrating,[10] organelle-targeting[11] and receptor-targeting[12] peptides to modulate their cellular uptake and intracellular localisation properties. Metal–peptide conjugates are commonly prepared from the coupling of a metal complex to a resin-bound, protected peptide, followed by peptide cleavage and deprotection to achieve site-selective functionalisation.[13] Also, selective post-modification of an unprotected peptide with a metal complex under mild and biocompatible conditions is highly attractive.[14] With our continued effort in the design of sulfhydryl-specific reagents,[14d,e,15] we report herein the design and synthesis of three near-infrared (NIR)-emitting cyclometallated iridium(III) polypyridine complexes modified with a heteroaromatic methylsulfone moiety $[Ir(bpz)_2(N^\wedge N)](PF_6)$ (Hbpz = benzo[*a*]phenazine; N^N = bpy-btz (**1**), bpy-mstp (**2**) and bpy-odz (**3**)) (Scheme 2) for the chemoselective modification of cysteine. The methylsulfone-free analogue $[Ir(bpz)_2(bpy\text{-}ph)](PF_6)$ (**4**) was also prepared for comparison. The development of NIR-emissive probes is highly important for biomedical imaging as luminescent probes with absorption and emission in the visible region (λ < 650 nm) are usually limited by short tissue penetration and interference by the strong

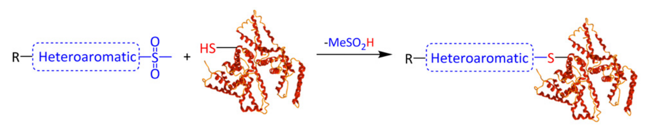

Scheme 1 Labelling of cysteine residues of proteins by heteroaromatic methylsulfones.

[a] Department of Chemistry, City University of Hong Kong, Tat Chee Avenue, Hong Kong, P. R. China. E-mail: bhkenlo@cityu.edu.hk
[b] State Key Laboratory of Terahertz and Millimetre Waves, City University of Hong Kong, Tat Chee Avenue, Kowloon, Hong Kong, P. R. China
[c] Laboratory for Synthetic Chemistry and Chemical Biology Limited, Units 1503 – 1511, 15/F, Building 17W, Hong Kong Science Park, New Territories, Hong Kong, P. R. China

† Electronic supplementary information (ESI) available. See DOI: https://doi.org/10.1039/d2cc02405e

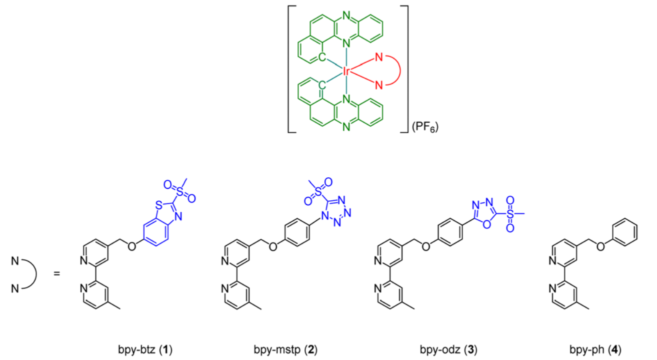

Scheme 2 Structures of complexes **1–4**.

autofluorescence background. Thus, the ligand Hbpz with a high degree of π-conjugation was selected as a cyclometallating ligand with the purpose of tuning the emission of the complexes to the NIR region. The synthetic procedures and characterisation data are included in the ESI.†

All the complexes displayed intense spin-allowed intraligand (^{1}IL) ($\pi \rightarrow \pi^*$) (N^N and bpz) absorption at *ca.* 275–410 nm and weaker spin-allowed metal-to-ligand charge-transfer (^{1}MLCT) (dπ(Ir) → π*(N^N and bpz)) absorption features at *ca.* 411–630 nm (Table S1 and Fig. S1, ESI†). The weaker absorption tailing beyond *ca.* 631 nm is assigned to spin-forbidden ^{3}MLCT (dπ(Ir) → π*(N^N and bpz)) transitions. Upon photoexcitation, all the complexes exhibited moderately intense and long-lived deep-red emission (Table 1 and Fig. S2, ESI†). The long emission lifetimes and insensitivity of emission properties to solvent polarity indicate that the emission originates from a predominant ^{3}IL ($\pi \rightarrow \pi^*$) (bpz) state. This is supported by the vibronically structured emission bands and long emission lifetimes (8.30–9.91 μs) in 77 K glass. Additionally, the $^1O_2$ generation quantum yields (Φ_Δ) of the complexes were determined in aerated MeOH using 1,3-diphenylisobenzofuran (DPBF) as a $^1O_2$ scavenger (Table 1). The Φ_Δ values of complexes **1–3** (0.77–0.89) were comparable to that of complex **4** (0.82), indicating that the methylsulfone moiety did not influence the photophysical and photochemical properties of the iridium(III) polypyridine unit.

Table 1 Photophysical data and $^1O_2$ generation quantum yields (Φ_Δ) of complexes **1–4**

Complex	Medium (*T*/K)	λ_{em}/nm[a]	τ_o/μs[b]	Φ_{em}[c]	Φ_Δ[d]
1	CH_2Cl_2 (298)	664	5.63	0.085	0.79
	CH_3CN (298)	668	3.26	0.044	
	Glass[e] (77)	663, 726 sh	8.30		
2	CH_2Cl_2 (298)	664	5.34	0.085	0.89
	CH_3CN (298)	668	3.46	0.048	
	Glass[e] (77)	663, 726 sh	9.91		
3	CH_2Cl_2 (298)	664	5.08	0.072	0.77
	CH_3CN (298)	668	3.23	0.044	
	Glass[e] (77)	663, 726 sh	9.40		
4	CH_2Cl_2 (298)	664	5.12	0.068	0.82
	CH_3CN (298)	668	3.44	0.052	
	Glass[e] (77)	663, 726 sh	9.22		

[a] λ_{ex} = 350 nm. [b] The lifetimes were measured at the emission maxima (λ_{ex} = 355 nm). [c] $[Ru(bpy)_3]Cl_2$ was used as a reference (Φ_{em} = 0.04 in aerated H_2O).[16] [d] $[Ru(bpy)_3]Cl_2$ was used as a reference (Φ_Δ = 0.73 in aerated MeOH).[17] [e] EtOH/MeOH (4 : 1, v/v).

The reactivity of the methylsulfone complexes **1–3** toward L-cysteine in aqueous solutions was analysed by reversed-phase high-performance liquid chromatography (RP-HPLC). The complexes (25 μM) were incubated with cysteine (250 μM) in potassium phosphate buffer (100 mM, pH 8.0)/DMF (4 : 1, v/v, 500 μL) containing tris(2-carboxyethyl)phosphine (TCEP) (750 μM) at 37 °C. Complexes **2** and **3** reacted rapidly with cysteine (< 5 min) to afford the iridium(III)–cysteine conjugates **2-Cys** and **3-Cys**, respectively, with reaction yields > 98% (Fig. S3, ESI†). However, it took much longer for complex **1** to complete the same reaction (2 h). The formation of products was confirmed by ESI-MS (Fig. S4, ESI†). The second-order rate constants (k_2) of the reaction of complexes **1**, **2** and **3** with cysteine were determined to be *ca.* 1.4, 83.6 and 1228.4 $M^{-1}\,s^{-1}$, respectively (Fig. S5, ESI†), which are similar to those of the corresponding free ligands (k_2 = 1.6, 79.5 and 1033.2 $M^{-1}\,s^{-1}$, respectively) (Fig. S6, ESI†). Thus, the metal complex cores did not substantially affect the reactivity of the heteroaromatic methylsulfone group, which is in line with the fact that there is a lack of π-conjugated linker between the two units. Although complex **3** displayed the highest reactivity toward cysteine, it was also more susceptible to hydrolysis (Fig. S7, ESI†). Thus, complex **2**, which exhibited a delicate balance of high reactivity and stability, was selected as a model complex for further studies.

Complex **2** was incubated with amino acids bearing reactive side-chains such as L-lysine, L-histidine and L-serine for 12 h under the same conditions mentioned above. No reactions were observed (Fig. S8, ESI†), illustrating the high chemoselectivity of the complex toward cysteine. Next, an epidermal growth factor receptor (EGFR)-targeting peptide modified with a cysteine residue at the N-terminus CYHWYGYTPQNVI (GE11)[18] was employed as a model for conjugation studies. Upon the incubation of GE11 (250 μM) and complex **2** (25 μM) in potassium phosphate buffer (100 mM, pH 8.0)/DMF (4 : 1, v/v, 500 μL) containing TCEP (750 μM) at 37 °C for 30 min, the production of the peptide conjugate **2-GE11** was confirmed by RP-HPLC and ESI-MS (Fig. S9 and S13, ESI†). Given the high reactivity, selectivity and stability of complex **2**, it was also conjugated to cysteine-modified endoplasmic reticulum-targeting peptide CKDEL (ER) and nuclear localisation sequence CPKKKRKV (NLS), and the proteins bovine serum albumin (BSA) and human serum albumin (HSA) to afford conjugates **2-ER**, **2-NLS**, **2-BSA** and **2-HSA**, respectively. All the conjugates were purified by RP- or size-exclusion HPLC, and their photophysical and photochemical properties were studied. Upon irradiation, the cysteine and peptide conjugates displayed moderately intense and long-lived emission and high Φ_Δ (0.61–0.86) (Table S2, ESI†), showing that the conjugation did not significantly perturb the photophysical and photochemical behaviour of the complexes. The emission maxima of **2-BSA** and **2-HSA** were blue-shifted, and their emission lifetimes were longer and quantum yields were higher than those of the cysteine and peptide conjugates, which are ascribed to the hydrophobic local environments of the complexes after conjugation to the protein

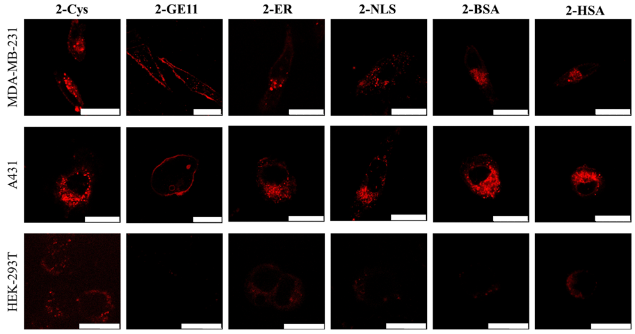

Fig. 1 LSCM images of MDA-MB-231, A431 and HEK-293T cells incubated with **2-Cys**, **2-GE11**, **2-ER**, **2-NLS**, **2-BSA** and **2-HSA** (10 μM, 4 h, λ_{ex} = 488 nm, λ_{em} = 650–750 nm). Scale bar = 25 μm.

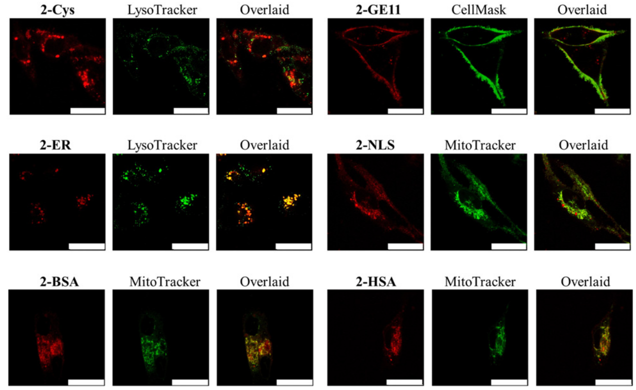

Fig. 2 LSCM images of MDA-MB-231 cells incubated with **2-Cys**, **2-GE11**, **2-ER**, **2-NLS**, **2-BSA** and **2-HSA** (10 μM, 4 h, λ_{ex} = 488 nm, λ_{em} = 650–750 nm) at 37 °C and then with an organelle stain (LysoTracker Green, 100 nM, 20 min, λ_{ex} = 488 nm, λ_{em} = 506–526 nm; MitoTracker Green, 100 nM, 20 min, λ_{ex} = 488 nm, λ_{em} = 506–526 nm; CellMask Deep Red, 5 μg mL^{-1}, 10 min, λ_{ex} = 635 nm, λ_{em} = 650–700 nm) at 37 °C. Scale bar = 25 μm.

molecules.[15d] The Φ_Δ values of the two protein conjugates (0.17 and 0.11) were smaller than those of the cysteine and peptide conjugates (0.61–0.86), which may be due to the entrapment of $^1O_2$ in the protein matrix, rendering it more difficult to diffuse out and react with DPBF.

The intracellular localisation properties of the cysteine, peptide and protein conjugates of complex **2** and the methylsulfone-free complex **4** were investigated by laser-scanning confocal microscopy (LSCM) using MDA-MB-231 (breast carcinoma), A431 (epidermoid carcinoma) and HEK-293T (normal human embryonic kidney) cells as models (Fig. 1 and Fig. S19, ESI†). In general, all six conjugates showed stronger luminescence signals in MDA-MB-231 and A431 cells than in HEK-293T cells (Fig. 1), but there was no noticeable difference for complex **4** (Fig. S19, ESI†). Incubation of MDA-MB-231 cells with **2-Cys** resulted in punctate cytoplasmic staining (Fig. 1). Very weak co-localisation with LysoTracker Green (Pearson's correlation coefficient (PCC) = 0.37) (Fig. 2) suggested that the conjugate was entrapped in the endosomes after uptake.[19] Notably, treatment of MDA-MB-231 cells with **2-GE11** gave rise to intense emission in the plasma membrane (Fig. 1) with strong co-localisation with CellMask Deep Red (PCC = 0.88) (Fig. 2). This is most likely resulted from the affinity of the GE11 peptide with EGFRs on the cell surface.[20] Cells incubated with **2-ER** and **2-NLS** showed intense emission in the lysosomal (PCC = 0.73) and mitochondrial (PCC = 0.82) regions, respectively, instead of the expected endoplasmic reticulum and nucleus. The localisation of **2-ER** in the lysosomes can be ascribed to the entrapment of the conjugate in these organelles, while the mitochondrial enrichment of **2-NLS** may be due to the cationic and lipophilic character of the conjugate.[14e] The perinuclear staining by the protein conjugates **2-BSA** and **2-HSA** in the cell lines (Fig. 1) suggests their localisation in the mitochondrial region, which was confirmed by co-staining experiments (Fig. 2). Complex **4** was also localised in the mitochondria of MDA-MB-231 cells (Fig. S19 and S20, ESI†).

The cytotoxicity of the six conjugates and complex **4** was studied by the 3-(4,5-dimethylthiazol-2-yl)-2,5-diphenyltetrazolium bromide (MTT) assay. All six conjugates showed relatively low cytotoxic activity toward the three cell lines in the dark ($IC_{50,dark}$ > 20 μM) after an incubation period of 4 h (Table 2).[21] However, upon irradiation (450 nm, 10 mW cm^{-2}) for 20 min, their cytotoxicity was substantially enhanced ($IC_{50,light}$ = 0.07–10.09 μM). Notably, the four conjugates **2-Cys**, **2-GE11**, **2-ER** and **2-NLS** displayed potent photocytotoxic activity toward cancerous MDA-MB-231 and A431 cells ($IC_{50,light}$ = 0.07–1.01 μM) with a photocytotoxicity index (PI, $IC_{50,dark}/IC_{50,light}$) > 20; the activity was much higher than that toward HEK-293T cells ($IC_{50,light}$ = 0.44–10.09 μM; PI > 2). These findings are attributable to the more efficient uptake of these four conjugates by the cancer cells than the normal HEK-293T cells. This was supported by the ICP-MS data, which showed that the iridium content in cancer cells (1.17–2.62 fmol per cell) was higher than in normal cells (0.13–0.32 fmol per cell) (Table S4, ESI†). In agreement with these results, the intracellular emission intensity of HEK-293T cells was much weaker than those of the two cancer cell lines (Fig. 1). Notably, **2-GE11** exhibited higher cancer-selective photocytotoxicity than the other conjugates, as the $IC_{50,light}$ values of this conjugate toward MDA-MB-231 (1.01 μM) and A431 cells (0.49 μM) were one and two orders of magnitude smaller than that toward HEK-293T cells (10.09 μM) (Table 2), which is also in agreement with the uptake data (Table S4, ESI†). The protein conjugates **2-BSA** and **2-HSA** showed higher dark cytotoxicity toward the two cancer cells than the normal cells. However, a similar trend was not observed in the photocytotoxicity, which is most likely due to a combined effect of the Φ_Δ, uptake efficiency and localisation. In comparison, the methylsulfone-free complex **4** exhibited very high dark and light cytotoxic activity toward the three cell lines ($IC_{50,dark}$ = 0.49–0.94 μM, $IC_{50,light}$ = 0.005–0.02 μM) (Table 2), which should be associated with its high uptake (Table S4, ESI†) and large Φ_Δ (Table 1). These results indicate that bioconjugation readily modulates the cellular uptake and the (photo)cytotoxic activity of the complexes.

In conclusion, we have developed cyclometallated iridium(III) polypyridine methylsulfone complexes featuring NIR emission, high reactivity and selectivity toward cysteine-bearing peptides and proteins. Bioconjugates modified with these complexes displayed different intracellular localisation properties. We believe that related transition metal methylsulfone complexes with both

Table 2 (Photo)cytotoxicity (IC_{50}) of the conjugates of complex **2** and the methylsulfone-free complex **4** toward MDA-MB-231, A431 and HEK-293T cells. The cells were first incubated with the conjugates or complex **4** in the dark for 4 h, then washed thoroughly with PBS, incubated in the dark or irradiated at 450 nm (10 mW cm^{-2}) for 20 min, and subsequently incubated in the dark for 24 h. Photocytotoxicity index (PI) = $IC_{50,dark}/IC_{50,light}$

	MDA-MB-231			A431			HEK-293T		
Compound	$IC_{50,dark}$/μM	$IC_{50,light}$/μM	PI	$IC_{50,dark}$/μM	$IC_{50,light}$/μM	PI	$IC_{50,dark}$/μM	$IC_{50,light}$/μM	PI
2-Cys	>20	0.07 ± 0.01	>286	>20	0.12 ± 0.01	>167	>20	0.44 ± 0.10	>45
2-GE11	>20	1.01 ± 0.08	>20	>20	0.49 ± 0.01	>41	>20	10.09 ± 1.85	>2
2-ER	>20	0.52 ± 0.07	>38	>20	0.25 ± 0.01	>80	>20	3.08 ± 0.10	>6
2-NLS	>20	0.11 ± 0.01	>182	>20	0.13 ± 0.01	>154	>20	1.27 ± 0.12	>16
2-BSA	46.21 ± 3.74	0.28 ± 0.06	165	28.36 ± 3.40	0.17 ± 0.01	167	49.65 ± 6.04	0.24 ± 0.06	207
2-HSA	53.05 ± 2.99	0.44 ± 0.09	121	24.91 ± 0.20	0.13 ± 0.01	192	74.90 ± 3.29	0.43 ± 0.07	174
4	0.69 ± 0.05	0.02 ± 0.005	35	0.49 ± 0.04	0.005 ± 0.001	98	0.94 ± 0.12	0.02 ± 0.008	47

absorption and emission in the NIR region (*e.g.*, by using extensively π-conjugated ligands and two-photon excitation techniques) can be designed as attractive sulfhydryl-specific reagents for bioconjugation.

We thank the Hong Kong Research Grants Council (Project No. CityU 11300019, CityU 11302820, CityU 11301121, T42-103/16-N, C7075-21GF and N_CityU104/21) for financial support. We also thank the funding support from "Laboratory for Synthetic Chemistry and Chemical Biology" under the Health@InnoHK Programme launched by Innovation and Technology Commission, The Government of Hong Kong SAR, P. R. China. L.H. and G.-X.X. acknowledge the receipt of a Postgraduate Studentship administered by City University of Hong Kong.

Conflicts of interest

There are no conflicts to declare.

References

1 (*a*) N. Stephanopoulos and M. B. Francis, *Nat. Chem. Biol.*, 2011, **7**, 876–884; (*b*) N. Krall, F. P. da Cruz, O. Boutureira and G. J. L. Bernardes, *Nat. Chem.*, 2016, **8**, 103–113.

2 (*a*) J. M. Chalker, G. J. L. Bernardes, Y. A. Lin and B. G. Davis, *Chem. Asian J.*, 2009, **4**, 630–640; (*b*) S. B. Gunnoo and A. Madder, *ChemBioChem*, 2016, **17**, 529–553; (*c*) F. Brotzel and H. Mayr, *Org. Biomol. Chem.*, 2007, **5**, 3814–3820.

3 D. Zhang, N. O. Devarie-Baez, Q. Li, J. R. Lancaster and M. Xian, *Org. Lett.*, 2012, **14**, 3396–3399.

4 (*a*) N. Toda, S. Asano and C. F. Barbas III, *Angew. Chem., Int. Ed.*, 2013, **52**, 12592–12596; (*b*) J. T. Patterson, S. Asano, X. Li, C. Rader and C. F. Barbas III, *Bioconjugate Chem.*, 2014, **25**, 1402–1407.

5 X. Chen, H. Wu, C.-M. Park, T. H. Poole, G. Keceli, N. O. Devarie-Baez, A. W. Tsang, W. T. Lowther, L. B. Poole, S. B. King, M. Xian and C. M. Furdui, *ACS Chem. Biol.*, 2017, **12**, 2201–2208.

6 H. F. Motiwala, Y.-H. Kuo, B. L. Stinger, B. A. Palfey and B. R. Martin, *J. Am. Chem. Soc.*, 2020, **142**, 1801–1810.

7 P. Zhou, J. Yao, G. Hu and J. Fang, *ACS Chem. Biol.*, 2016, **11**, 1098–1105.

8 (*a*) B. Albada and N. Metzler-Nolte, *Chem. Rev.*, 2016, **116**, 11797–11839; (*b*) S. M. Meier-Menches and A. Casini, *Bioconjugate Chem.*, 2020, **31**, 1279–1288; (*c*) L. Holden, C. S. Burke, D. Cullinane and T. E. Keyes, *RSC Chem. Biol.*, 2021, **2**, 1021–1049.

9 (*a*) K. K.-W. Lo, *Acc. Chem. Res.*, 2015, **48**, 2985–2995; (*b*) Y. You, *Curr. Opin. Chem. Biol.*, 2013, **17**, 699–707; (*c*) H. Huang, S. Banerjee and P. J. Sadler, *ChemBioChem*, 2018, **19**, 1574–1589.

10 (*a*) C. A. Puckett and J. K. Barton, *J. Am. Chem. Soc.*, 2009, **131**, 8738–8739; (*b*) A. Byrne, C. S. Burke and T. E. Keyes, *Chem. Sci.*, 2016, **7**, 6551–6562; (*c*) S. Ji, X. Yang, X. Chen, A. Li, D. Yan, H. Xu and H. Fei, *Chem. Sci.*, 2020, **11**, 9126–9133.

11 (*a*) A. Martin, A. Byrne, C. S. Burke, R. J. Forster and T. E. Keyes, *J. Am. Chem. Soc.*, 2014, **136**, 15300–15309; (*b*) C. S. Burke, A. Byrne and T. E. Keyes, *J. Am. Chem. Soc.*, 2018, **140**, 6945–6955; (*c*) C. S. Burke, A. Byrne and T. E. Keyes, *Angew. Chem., Int. Ed.*, 2018, **57**, 12420–12424.

12 (*a*) X. Ma, J. Jia, R. Cao, X. Wang and H. Fei, *J. Am. Chem. Soc.*, 2014, **136**, 17734–17737; (*b*) K. Vellaisamy, G. Li, W. Wang, C.-H. Leung and D.-L. Ma, *Chem. Sci.*, 2018, **9**, 8171–8177; (*c*) W. Wang, K.-J. Wu, K. Vellaisamy, C.-H. Leung and D.-L. Ma, *Angew. Chem., Int. Ed.*, 2020, **59**, 17897–17902.

13 (*a*) N. Y. Sardesai, K. Zimmermann and J. K. Barton, *J. Am. Chem. Soc.*, 1994, **116**, 7502–7508; (*b*) M. P. Fitzsimons and J. K. Barton, *J. Am. Chem. Soc.*, 1997, **119**, 3379–3380; (*c*) F. Noor, A. Wüstholz, R. Kinscherf and N. Metzler-Nolte, *Angew. Chem., Int. Ed.*, 2005, **44**, 2429–2432; (*d*) A. H. Day, M. H. Übler, H. L. Best, E. Lloyd-Evans, R. J. Mart, I. A. Fallis, R. K. Allemann, E. A. H. Al-Wattar, N. I. Keymer, N. J. Buurma and S. J. A. Pope, *Chem. Sci.*, 2020, **11**, 1599–1606; (*e*) D. Truong, N. Y. S. Lam, M. Kamalov, M. Riisom, S. M. F. Jamieson, P. W. R. Harris, M. A. Brimble, N. Metzler-Nolte and C. G. Hartinger, *Chem. Eur. J.*, 2022, **28**, e202104049.

14 (*a*) H.-Y. Shiu, H.-C. Chong, Y.-C. Leung, T. Zou and C.-M. Che, *Chem. Commun.*, 2014, **50**, 4375–4378; (*b*) A. Leonidova, V. Pierroz, L. A. Adams, N. Barlow, S. Ferrari, B. Graham and G. Gasser, *ACS Med. Chem. Lett.*, 2014, **5**, 809–814; (*c*) T. Wang, N. Zabarska, Y. Wu, M. Lamla, S. Fischer, K. Monczak, D. Y. W. Ng, S. Rau and T. Weil, *Chem. Commun.*, 2015, **51**, 12552–12555; (*d*) L. C.-C. Lee, A. W.-Y. Tsang, H.-W. Liu and K. K.-W. Lo, *Inorg. Chem.*, 2020, **59**, 14796–14806; (*e*) P. K.-K. Leung, L. C.-C. Lee, T. K.-Y. Ip, H.-W. Liu, S.-M. Yiu, N. P. Lee and K. K.-W. Lo, *Chem. Commun.*, 2021, **57**, 11256–11259.

15 (*a*) K. K.-W. Lo, D. C.-M. Ng and C.-K. Chung, *Organometallics*, 2001, **20**, 4999–5001; (*b*) K. K.-W. Lo, C.-K. Chung, D. C.-M. Ng and N. Zhu, *New J. Chem.*, 2002, **26**, 81–88; (*c*) K. K.-W. Lo, W.-K. Hui, D. C.-M. Ng and K.-K. Cheung, *Inorg. Chem.*, 2002, **41**, 40–46; (*d*) K. K.-W. Lo, C.-K. Chung, T. K.-M. Lee, L.-H. Lui, K. H.-K. Tsang and N. Zhu, *Inorg. Chem.*, 2003, **42**, 6886–6897.

16 K. Suzuki, A. Kobayashi, S. Kaneko, K. Takehira, T. Yoshihara, H. Ishida, Y. Shiina, S. Oishi and S. Tobita, *Phys. Chem. Chem. Phys.*, 2009, **11**, 9850–9860.

17 D. Garcìa-Fresnadillo, Y. Georgiadou, G. Orellana, A. M. Braun and E. Oliveros, *Helv. Chim. Acta*, 1996, **79**, 1222–1238.

18 Z. Li, R. Zhao, X. Wu, Y. Sun, M. Yao, J. Li, Y. Xu and J. Gu, *FASEB J.*, 2005, **19**, 1978–1985.

19 A. K. Varkouhi, M. Scholte, G. Storm and H. J. Haisma, *J. Controlled Release*, 2011, **151**, 220–228.

20 (*a*) I. Genta, E. Chiesa, B. Colzani, T. Modena, B. Conti and R. Dorati, *Pharmaceutics*, 2018, **10**, 2; (*b*) M. A. Sandoval, B. R. Sloat, D. S. P. Lansakara-P, A. Kumar, B. L. Rodriguez, K. Kiguchi, J. DiGiovanni and Z. Cui, *J. Controlled Release*, 2012, **157**, 287–296.

21 The cytotoxicity data for longer incubation times (24 and 48 h) are included in the ESI.†